Atomic-scale visualization of surface segregation and ordering of Pt in dilute Cu(Pt) alloy under hydrogen atmosphere

Zhilu Liang[1+], Dongxiang Wu[1+], Xianhu Sun[1], Xiaobo Chen[1], Dmitri N. Zakharov[2], Judith C Yang[2], Guangwen Zhou[1*]

[1]Materials Science and Engineering Program and Department of Mechanical Engineering, State University of New York, Binghamton, New York 13902, USA
[2]Center for Functional Nanomaterials, Brookhaven National Laboratory, Upton, New York 11973, USA

ABSTRACT

Surface segregation is a common phenomenon in alloys exposed to reactive atmospheres, yet the atomic mechanisms underlying surface structure and composition dynamics remains largely unexplored. Using a combination of environmental transmission electron microscopy observations and atomistic modeling, here we report the surface segregation process of Pt atoms in a dilute Pt(Cu) alloy and determine the distribution of Pt atoms at both atomically flat and stepped surfaces of the Pt(Cu) alloy at elevated temperature and in a hydrogen gas atmosphere. Through directly probing Pt segregation, we find that Pt atoms segregated on the (100) surface exhibit a p(2×2) ordering, with ~25% Pt occupancy. In contrast, on the stepped (410) surface, hydrogen adsorption induces Pt segregation, initially occurring at the step edges, which then expands to the terrace sites upon increased hydrogen coverage, resulting in an ordered distribution of segregated Pt atoms with ~22% occupancy. These observations offer mechanistic insights into the structure and composition dynamics of the topmost atomic layer of the alloy in response to environmental stimuli and hold practical implications for the design and optimization of catalysts based on Pt group metals.

+ These authors contributed equally to the work

*Corresponding author: gzhou@binghamton.edu

1. INTRODUCTION

Surface segregation in alloys is a critical phenomenon that profoundly influences the performance and stability of materials across various industrial applications[1-3]. Gaining a fundamental understanding of the mechanisms driving surface segregation is essential for optimizing material properties, particularly when exposed to reactive atmospheres. In binary alloys, the segregation of one component to the surface can significantly affect catalytic activity, corrosion resistance, and mechanical strength. The presence of reactive environments, such as oxidizing or reducing gases, further complicates these dynamics by altering the stability and distribution of alloying elements[4-8]. Despite its importance, achieving atomic-scale understanding of surface segregation in alloys under reactive conditions is challenging due to the limitations of most experimental tools in probing the topmost surface regions. Nevertheless, this fundamental knowledge is crucial for advancing technologies in fields like heterogeneous catalysis, where surface reactions are central to catalytic efficiency[9-13], and materials science, where alloy composition and structure dictate performance under operational conditions[14-17]. Investigating these phenomena provides a deeper understanding of how to design and engineer alloys with tailored properties, leading to more efficient, durable, and cost-effective materials for a wide range of applications.

Bimetallic alloys often exhibit significantly enhanced catalytic performance and long-term stability compared with their constituent metals due to ligand/electronic and geometric/strain effects[18-20]. For instance, one of the extreme cases is to disperse a catalytically active noble metal (such as Pt) in more inert host metals (e.g., Cu, Ni, Fe) at the single-atom limit, creating single atom alloys (SAAs)[21-29]. For example, Sykes et al demonstrated that a low coverage (<0.05 monolayer) of Pt or Pd deposited on Cu(111) forms a SAA that that exhibits activity in the dissociation of H_2 and the spillover of H to Cu sites for hydrogenation reactions[30-31]. Although such SAAs have been extensively studied[32-43], there is still a lack of understanding regarding how the alloy behaves dynamically under the reaction conditions of elevated temperature and reactive gases. Additionally, the study of SAAs has predominantly focused on well-defined single crystals[44-45]. However, even the surface of a single crystal is still far from being perfect, containing numerous atomic defects. For instance, atomic steps, which are

common defects on crystal surfaces, may behave differently from a flat surface due to reduced coordination at step sites, and significantly alter the surface distribution of noble metal atoms.

To evaluate the surface segregation phenomena in alloys, it is crucial to consider their stability and response under reaction conditions. Factors such as the presence of gases and elevated temperatures can induce elemental segregation, leading to changes in surface composition as well as surface restructuring and redistribution of noble metal atoms[4]. Surface-sensitive spectroscopic techniques like X-ray photoemission spectroscopy (XPS) are commonly employed to investigate the surface composition of alloys[46-48]. However, these techniques are not structure sensitive and cannot unambiguously differentiate between surface and subsurface layers due to the temporal and spatial superposition of signals originating from multiple atomic layers. Alternatively, surface science tools such as ion scattering spectroscopy and low-energy electron diffraction provide surface-specific information on surface composition and structure when working in tandem, However, they are limited to ultrahigh vacuum (UHV) conditions, lack spatial resolution, and are prone to averaging information. On the other hand, scanning tunneling microscopy is one of the few techniques capable of obtaining atomic-site-selective quantitative information. Nevertheless, it cannot be readily used at elevated temperatures and in reactive gas atmospheres, which are often required to drive surface segregation and restructuring in catalytic reactions.

In contrast, transmission electron microscopy (TEM) overcomes many of the limitations faced by traditional surface science tools, providing atomic-scale insights into surface segregation phenomena. Recent advancements in TEM now allow for temperature-resolved, pressure-resolved, and time-resolved imaging of gas-surface reaction dynamics. By introducing reactive gases into the sample area in the TEM column, TEM can capture the atomic-scale structural evolution from the outermost surface layer to deeper subsurface regions. This capability is crucial for understanding alloy segregation dynamics, as the surface of the material can undergo significant changes during interactions with reactive environments. The ability to observe these dynamic processes in real time allows for a more comprehensive understanding

of how surface segregation evolves under practical conditions, enhancing our knowledge of material behavior and performance.

In this work, we employ in situ environmental transmission electron microscopy (TEM) to investigate the surface and composition dynamics within the topmost atomic layer of a dilute Cu(Pt) alloy under reactive and high-temperature conditions. This approach leverages the unique capabilities of environmental TEM to provide atomic-scale insights into surface segregation dynamics. Complementing these observations, coordinated density-functional theory (DFT) modeling is used to enhance the understanding of the experimental results by offering mechanistic insights into the atomic processes observed. The synergy between in-situ TEM imaging and DFT modeling allows for a detailed analysis of the dynamic segregation behavior of the alloy, bridging the gap between the experimental observations and theoretical predictions. The results reported here are highly relevant to a wide range of material systems, properties, and reactions, including metallurgy, nanostructure synthesis, redox reactions, and heterogeneous catalysis.

2.EXPERIMENTAL AND COMPUTATIONAL METHODS

2.1 Sample preparation and in-situ TEM imaging

Our in-situ TEM experiments were performed using a dedicated field-emission environmental TEM (FEI Titan 80-300) equipped with an objective lens corrector and operated at 300 kV. Cu-5at.% Pt(100) single-crystal thin films, with a normal thickness of ~50 nm, were grown on NaCl(100) by electron beam co-evaporation of Cu and Pt. The alloy composition was controlled by adjusting the evaporation rates of the two electron guns. The grown Cu(Pt) alloy films were then transferred from the NaCl(100) substrate by floatation in deionized water, washed, and mounted on a TEM grid, and loaded onto a TEM heating holder. The as-loaded Cu(Pt) films underwent annealing inside the TEM at 600°C and under a H_2 gas flow of ~1×10^{-2} Torr to remove any native oxides present. The complete removal of oxide and surface cleanliness was confirmed by electron diffraction and electron energy loss spectroscopy. During annealing, holes and tears with faceted edges formed in the thin film, a process akin to

the mechanical cleavage of single crystals in vacuum. The freshly generated surface facets are atomically clean and ideal for cross-sectional high-resolution TEM (HRTEM) observations of Pt surface segregation induced structural changes in a H_2 gas atmosphere. To mitigate potential artifacts from electron-beam irradiation that could affect TEM results, the electron beam was blanked during the H_2 annealing process and unblanked only when acquiring TEM images. Additionally, the electron beam effect was carefully assessed by adjusting imaging condition in one area and then moving to a neighboring, fresh area for HRTEM imaging.

2.2 HRTEM image simulations

HRTEM image simulations were performed using the JEMS software with the multi-slice method. The simulation parameters were carefully adjusted to match the experimental conditions, including an accelerating voltage of 300 keV, spherical aberration of -0.03 mm, defocus, and specimen thickness. Density functional theory (DFT)-relaxed atomic structure models of the Cu(Pt) SAAs were used as the input files for HRTEM image simulations.

2.3 DFT calculations

DFT calculations were performed using the Vienna ab initio simulation package (VASP)[49-51] and PW91 Generalized Gradient Approximation (GGA)[52]. The projector-enhanced wave (PAW) potential was used to describe electron-electron exchange and core-electron potential[53]. The cut-off energy of the plane wave was set to 400 eV for all the calculations. Based on the Monkhorst-Pack grids, the (4×4×1) K-point meshes were applied to the integration of the Brillouin area[54]. The surface model was composed of five atomic layers of (2×2) repeated slabs, in which the bottom two layers were fixed at their bulk crystal positions, and all the other atoms were free to relax until the maximum force acting on each atom was less than 0.015 eV/Å.

The average binding energy of the surface as a function of H coverage was calculated using $E = \frac{1}{N_{\mathrm{H}}}\left(E_{\mathrm{tot}} - E_{\mathrm{p}} + N_{\mathrm{Cu}}E_{\mathrm{Cu}} - N_{\mathrm{Pt}}E_{\mathrm{Pt}} - N_{\mathrm{H}}E_{\mathrm{H}}\right)$, where E_{tot} is the total energy of the H/Cu(Pt) system, E_{P} is the energy of the pristine Cu structure, N_{Cu}, N_{Pt} and N_{H} are the differences in the number of Cu, Pt, and H atoms, respectively, in the H/Cu(Pt) and pure Cu systems, and E_{Cu}, E_{Pt}, and E_{H} are the energies of a single Cu, Pt, and H atom, respectively. Furthermore, to enable a comparison of H adsorption of on both the terrace and steps, the H

adsorption energy, E_{ads}, is determined using the equation $E_{\mathrm{ads}} = \frac{1}{N_{\mathrm{H}}}(E_{\mathrm{tot}} - E_0 - N_{\mathrm{H}}E_{\mathrm{H}})$, where E_0 is the energy of the pristine surface. To describe the segregation energy of Pt at the surface, the formula, $E_{\mathrm{seg}} = \frac{1}{N_{\mathrm{a}}}(E_{\mathrm{sur}} - E_{\mathrm{ref}})$, was used, where E_{sur} is the total energy of the Cu(Pt) system with Pt segregation at the surface, E_{ref} is the system energy of the original Cu(Pt) structure, and N_{a} is the number of Pt atoms segregated at the surface. All atomic structures were visualized using the Visualization for Electronic and Structure Analysis (VESTA).

3. RESULTS

High-resolution (HR) TEM imaging mode was employed to image the segregation phenomena within a dilute Cu(Pt) solid solution under the influence of a H_2 atmosphere and at elevated temperatures. The presence of H_2 gas served a dual purpose: it prevented surface oxidation of the alloy while also simulating conditions highly relevant to hydrogenation reactions, crucial in the production of both bulk and fine chemicals. Pt-based catalysts are commonly used in hydrogenation reactions to activate the chemical reaction between H_2 and other compounds. Employing in-situ TEM enabled us to spatially resolve surface segregation on both flat and stepped surfaces. Our observations reveal that surface segregation of Pt in the Cu(Pt) solid solution, induced by H adsorption, leads to the formation of SAAs. Notably, this mechanism diverges from the conventional surface deposition route for SAA formation[55-56]. Additionally, our observations show the pronounced influence of atomic steps in promoting Pt surface segregation, resulting in a higher surface concentration of Pt compared to atomically flat surfaces.

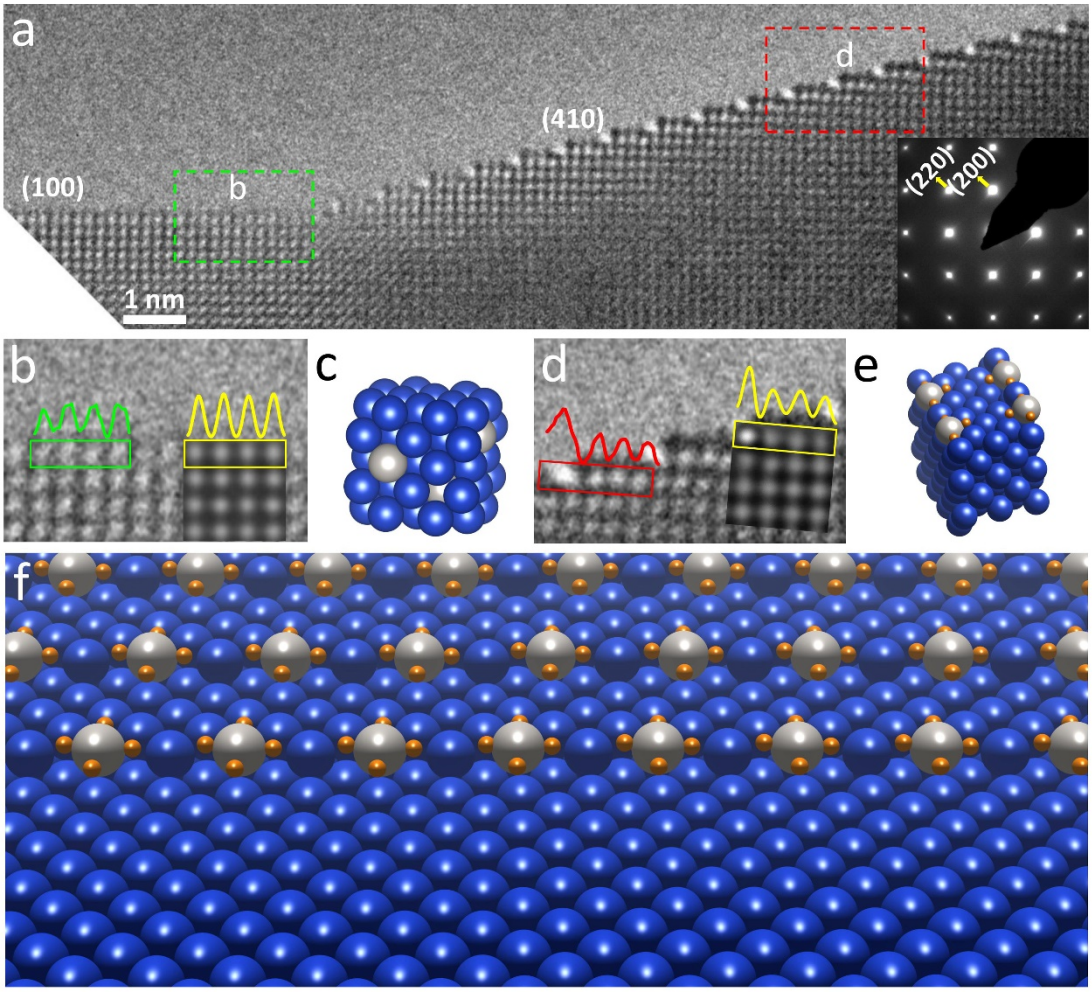

Fig. 1: (a) HRTEM image of the intersection region comprising (100) and stepped (410) surface facets, obtained by annealing the Cu-5 at.%Pt(100) film at 600°C and 1×10^{-2} Torr of H_2 flow. The inset is an FFT diffractogram of the HRTEM. (b) Enlarged view and intensity profile along the topmost layer of the (100) surface region marked with the green dashed box in (a). The yellow inset is a simulated HRTEM image and intensity profile of the topmost layer based on the DFT-relaxed (100) structure model in (c). (d) Zoomed-in view and intensity profile along the topmost layer of the stepped (410) facet region marked by the red dashed box in (a). The yellow inset is a simulated HRTEM image and intensity profile of the topmost layer of the DFT-relaxed (410) structure model in (e). (f) Schematic illustrating the disparity between the (100) and (410) facets: the (100) facet exhibits an absence of H adsorption and Pt segregation, whereas the (410) facet shows preferential H adsorption and Pt segregation occurring at the step edge.

Practically relevant catalytically active surfaces often exhibit a high density of atomic defects that function as active sites for bond-breaking and bond-making. However, systematically examining such surface defects experimentally can be challenging, especially when they lack order or regularity. High Miller index surfaces, characterized by flat low-Miller-

index terraces separated by atomic height steps, offer a pathway to explore these features. Fig. 1(a) illustrates an HRTEM image of the intersection region of the (100) and (410) facets. This morphology is formed by annealing the Cu-5at.%Pt(100) film at 600°C under a H_2 flow of 1×10^{-2} Torr. The (100) facet is atomically flat, while the (410) surface facet exhibits the stepped morphology composed of a sequence of four-atom-wide (100) terraces separated by periodic monoatomic steps with the (110) microfacet character. The bottom-right inset in Fig. 1(a) is a fast Fourier transform (FFT) diffractogram of the HRTEM image, which can be indexed well with the Cu lattice. This indicates the solid-solution nature of the Cu(Pt) alloy, confirming the homogeneous distribution of Pt atoms within the bulk of the Cu film.

Fig. 1(b) is a zoom-in view of the (100) flat surface region marked by the green dashed box in Fig. 1(a). The intensity profile along the topmost layer reveals relatively uniform image contrast among the atom columns from the topmost surface layer to the deeper atom layers. This uniform contrast suggests the absence of discernible surface segregation of Pt. This observation is further supported by the simulated HRTEM image (inset in Fig. 1(b)), which was obtained using a DFT-relaxed structure model of the Cu(Pt) solid solution (Fig. 1(c)). Fig. 1(d) shows an enlarged HRTEM view of the (410) facet region, as delineated by the red dashed box in Fig. 1(a). Here, the atom columns at the step edge exhibits ~50% stronger image intensity compared to the adjacent atom columns in the terrace. This indicates the preferential segregation of Pt atoms to the step edges rather than the terraces, as confirmed by image simulations described later.

Prior investigations on single crystals of Cu-Pt alloys under UHV annealing conditions have demonstrated a tendency for surface segregation of Cu induced by its lower surface energy relative to Pt[57-60]. However, the observation of Pt atoms segregating to the step edges in the (410) facet under the H_2 atmosphere represents a notable departure from the pristine surface behavior of the Cu-Pt alloy. This difference points to the significant influence of H adsorption in driving the segregation of Pt atoms towards the step edges, in line with the high dissociation barriers of H_2 molecules on Cu surfaces[61]. Notably, atomic H bonds weakly to Cu surfaces and desorbs from them at temperatures exceeding 80°C[62]. On the contrary, Pt surfaces are known

to facilitate the dissociation of H_2 molecules into atomic H, and Pt atoms exhibit a pronounced affinity toward H[63-65].

Fig. 1(e) depicts the DFT minimum-energy structure of a (410) surface model, comprising alternate Cu and Pt atoms (i.e., 50% of Pt) at the step edge. Our DFT calculations reveal that H atoms adsorb stably to the bridge sites adjacent to segregated Pt atoms in the step edge. The inset in Fig. 1(d) presents a simulated HRTEM image obtained using the DFT-relaxed structure model in Fig. 1(e). Intensity profile analysis of the simulated image indicate that the image intensity for the Cu/Pt atom columns in the step edge is ~50% stronger than that of the adjacent Cu atom columns in the terrace, consistent with the intensity profile of the experimental HRTEM image. Therefore, H adsorption along the step edge results in Pt segregation at the step edge with alternating occupation of Cu atoms by Pt atoms. Fig. 1(f) schematically illustrates the key distinction between the (100) and (410) facets. The (100) facet lacks H adsorption and Pt segregation, whereas the (410) facet displays the affinity for H adsorption along with Pt segregation within the step edge.

Fig. 2(a) displays an HRTEM image of the intersection region of the (100) and (410) facets following the continued H_2 annealing at 600°C under the H_2 flow of 1×10^{-2} Torr. Notably, certain atom columns within the outermost layer of the (100) facet exhibit brighter image contrasts, indicating the segregation of Pt atoms to the topmost surface due to H adsorption. Fig. 2(b) provides a zoomed-in view of the (100) region marked by the green dashed box in Fig. 2(a), where the intensity profile reveals the stronger image intensity of a single atom column compared to its adjacent counterparts. The yellow inset in Fig. 2(b) is a simulated HRTEM image derived from the DFT-relaxed structure (Fig. 2(c)), featuring a surface segregated Pt atom with H adsorption occurring at the hollow sites adjacent to the segregated Pt. The intensity profile analysis of the simulated image indicates that the image intensity for the atom column containing the segregated Pt is ~50% stronger than that for the adjacent Cu atom columns, consistent with the intensity profile observed in the experimental HRTEM image in Fig. 2(b).

Fig. 2(d) presents a zoomed-in view of the (410) facet region marked by red dashed box in Fig. 2(a). The intensity profile taken along the topmost terrace layer reveals that not only the

atom column at the step edge but also the atom column in the middle of the terrace exhibit similarly stronger image intensity compared to the atom column in between. Their difference in image intensity suggests the surface segregation of Pt atoms to every other atom column in the stepped facet upon progressive H adsorption. Fig. 2(e) shows a DFT minimum-energy structure of the (410) surface model, featuring an alternate substitution of Pt atoms (i.e., 50% Pt) at both the step edge and the second nearest neighbors in the terrace. Our DFT calculations show that the hollow and bridge sites adjacent to segregated Pt atoms in the step edge and the hollow sites next to the segregated Pt in the terrace are favorable for stable H adsorption. The yellow inset in Fig. 2(d) is a simulated HRTEM image obtained using the DFT-relaxed structure model in Fig. 2(e). Both the experimental and simulated HRTEM images indicate that the image intensity for the step-edge atom column (atom column 1) is ~50% stronger than atom column 2, as marked in Fig. 2(d). Furthermore, the images reveal the absence of Pt segregation to the fourth atom column, which exhibits the weakest image intensity. This observation is also consistent with the DFT modeling in Fig. 4(i), which suggests that Pt segregation to the fourth atom column is energetically unfavorable due to its close proximity to the ascending step on the right, already populated with segregated Pt and H.

Therefore, the progressive accumulation of adsorbed H along the step edge and in the terrace results in Pt segregation not only at the step edge but also to the terrace region. Fig. 2(f) schematically depicts this trend, where the H adsorption in the local areas of the (100) facet results in the segregation of isolated Pt atoms in the surface. By contrast, the stronger H affinity of the (410) facet results in the population of H adsorption from the step edge to the terrace region. This leads to the expansion of Pt segregation from the step edge to certain areas within the terrace.

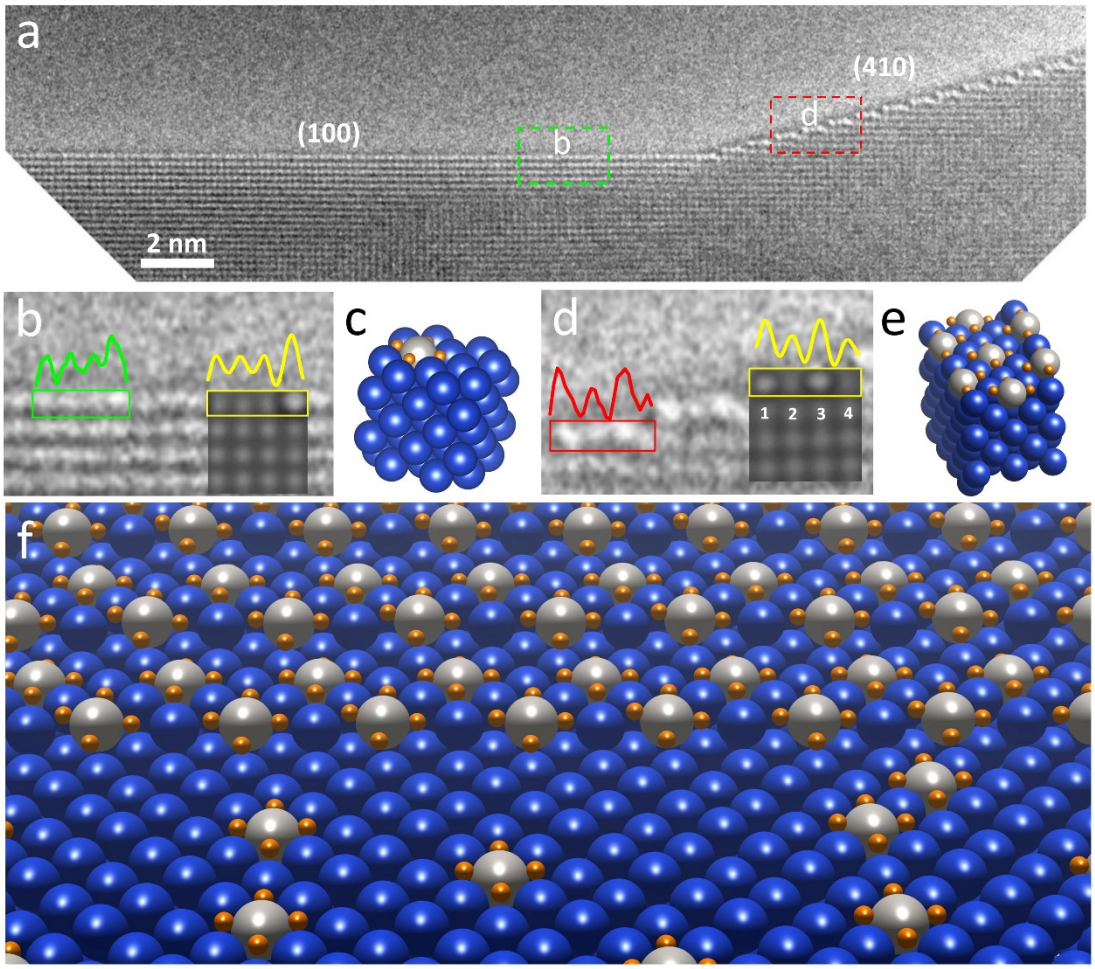

Fig. 2: (a) HRTEM image of the (100) and (410) facets after a longer period of H_2 annealing of the Cu-5at.%Pt alloy at 600°C and 1×10^{-2} Torr of H_2 flow. (b) Enlarged view and intensity profile along the topmost layer of the (100) surface region marked with the green dashed box in (a). The inset depicts a simulated HRTEM image and intensity profile of the topmost layer based on the DFT-relaxed (100) structure model in (c). (d) Zoomed-in view and intensity profile along the topmost layer of the stepped (410) facet region marked by the dashed red box in (a). The inset represents a simulated HRTEM image and intensity profile of the topmost layer. (e) DFT-relaxed (410) structures of H adsorption and Pt segregation along the step edge and within the terrace. (f) Schematic illustrating the difference between the (100) and (410) facets upon incremental H adsorption: H adsorption in local areas results in the surface segregation of isolated Pt atoms in the (100) facet, whereas on the (410), the accumulation of adsorbed H prompts Pt segregation to extend from the step edge to certain regions within the terrace.

Fig. 3(a) presents an HRTEM image of the (100) and (410) facets after an additional prolonged H_2 annealing period of at 600°C and 1×10^{-2} Torr H_2. Notably, the entire outermost layer of the (100) facet has now transformed into a superlattice structure, exhibiting alternating strong and weak image contrasts among the atom columns. Fig. 3(b) shows a zoomed-in view of the (100) region marked by the green dashed box in Fig. 3(a). Here, the intensity profile

analysis reveals a roughly 50% difference in image intensity between adjacent atom columns. In Fig. 3(b), the yellow inset depicts a simulated HRTEM image obtained using a DFT-relaxed structure of the p(2×2) ordering of segregated Pt atoms in the (100) surface. As depicted in Fig. 3(c), the p(2×2) ordering involves H adsorption taking place at the hollow sites adjacent to segregated Pt. Further intensity profile analysis of the simulated image indicates that the image intensity of the Cu/Pt columns is ~50% stronger than that of the adjacent Cu atom columns, matching the intensity profile observed in the experimental HRTEM image in Fig. 3(b).

Fig. 3(d) illustrates a magnified view of the (410) stepped facet region marked with the red dashed box in Fig. 3(a). The intensity profile analysis along the topmost terrace layer reveals that the atom columns at the step edge and in the middle of the terrace (i.e., atom columns 1 and 3, as marked in Fig. 3(d)) exhibit similar image intensities, which are ~30% stronger than the atom column 2. This observation suggests a surface segregation of more Pt atoms towards atom column 2, as the difference in image intensity between atom columns 1-3 decreases to ~20%, contrasting with that in Figs. 2(d, e). Notably, the image intensity for atom column 4 adjacent to the ascendant step edge is ~ 50% weaker than columns 1 and 3, akin to the difference observed in Fig. 3(b) between the Cu/Pt and Cu columns, indicating the absence of Pt segregation toward atom column 4. Fig. 3(e) corresponds to the DFT minimum-energy structure of the (410) surface model, featuring ordered distribution of segregated Pt atoms in the terrace. This arrangement entails alternating substitution of Pt atoms (i.e., 50% of Pt occupancy) at both the step edge and the atom column situated in the middle of the terrace. Fig. 3(f) depicts an alternative DFT-relaxed Pt-segregated structure of the (410) facet, featuring one Pt substitution for every four Cu atoms (i.e., 25% Pt) in the step edge and adjacent two atom columns in the terrace. Although this structure exhibits a slightly higher segregation energy compared to the configuration in Fig. 3(e), the difference is minimal. Neither of these Pt-segregated structures alone provides a satisfactory match with the experimental HRTEM image. This suggests the expansion of the two Pt-segregated structures depicted in Figs. 3(e, f). The yellow inset in Fig. 3(d) depicts a simulated HRTEM image obtained using a 1:1 combination of the two Pt-segregated structures depicted in Figs. 3(e, f). This combination results in ~ 22% Pt occupancy

within the stepped region by averaging the Pt content in all the four atom columns of the terrace and yields the best match with the experimental HRTEM images. Consequently, the increased coverage of adsorbed H within the terrace area of the stepped facet results in more Pt segregation to the terrace. Fig. 3(g) schematically illustrates the resulting Pt segregation: prolonged exposure to H_2 leads to increased H adsorption by the (100) facet, resulting in the formation of a p(2×2) pattern of segregated Pt atoms, occupying ~25% of the surface sites. In contrast, although the step edges in the (410) stepped facet are more favorable for H adsorption and Pt segregation compared to the flat (100) facet, the atom columns neighboring the ascending steps do not exhibit Pt segregation. This absence of Pt segregation is attributed to the high concentration of H and Pt along the ascending steps, thereby resulting in ~ 22% Pt occupancy of the surface sites within the (410) stepped facet, similar to that observed for the flat (100) facet.

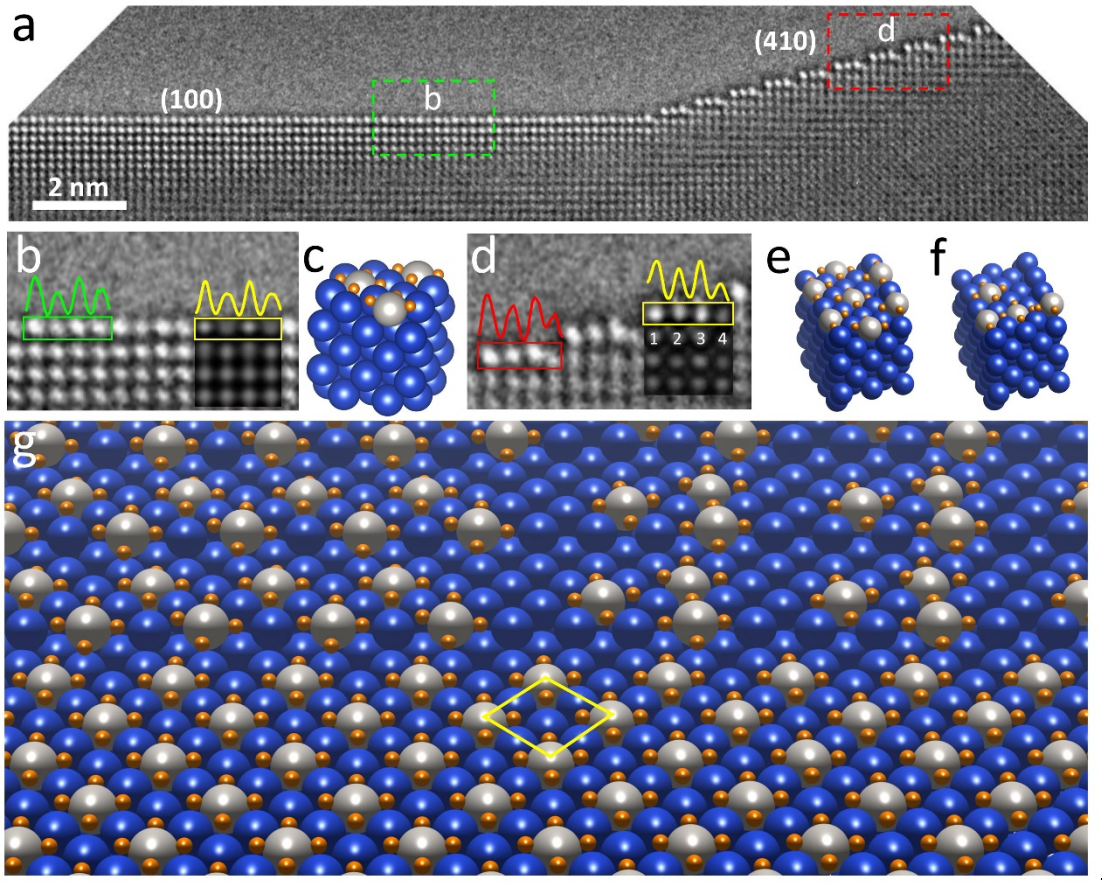

Fig. 3: (a) HRTEM image of the (100) and (410) facets after an extend period of the H_2 annealing of the Cu-5at.%Pt alloy at 600°C and 1×10^{-2} Torr of H_2 flow. (b) Enlarged view and intensity profile along the

topmost layer of the (100) surface region marked with the green dashed box in (a). The inset is a simulated HRTEM image and intensity profile of the topmost layer. (c) DFT-relaxed (100) structure consisting of p(2×2) ordering of Pt atoms. (d) Zoomed-in view and intensity profile along the topmost layer of the stepped (410) facet region marked by the dashed red box in (a). The inset is a simulated HRTEM image and intensity profile of the topmost layer. (e, f) DFT-relaxed (410) structure models showing the two competing surface structures from Pt segregation to the terrace. (g) Schematic illustrating the difference between the (100) and (410) surfaces upon the population of adsorbed H: p(2×2) ordering (marked by the yellow box) of the segregated Pt on the (100) facet, and the co-existing two ordering arrangements of segregated Pt atoms within the terraces of the (410) stepped facet.

To provide further additional support to the in-situ TEM observations described above, we performed DFT modeling to investigate the effect of H adsorption on inducing surface segregation of Pt on both the (100) terrace and the step edge. As illustrated in Fig. 4(a), Pt atoms are initially positioned at the lattice sites directly beneath the surface layer. Our DFT calculations for the pristine surface reveal that the segregation of Pt to both the step edge and the terrace leads to an increase in system energy. This suggests that Pt surface segregation is energetically unfavorable, consistent with previous experimental measurements[57, 59, 66] and computational modeling results[67-68]. Subsequently, we compare H adsorption at the terrace and step edge, revealing that H adsorption at the hollow site near the subsurface Pt along the step edge is more energetically favorable than at the hollow site above the sub-surface Pt in the (100) terrace, as depicted in Fig. 4(b). This trend is further supported by the DFT computation of Pt surface segregation upon the adsorption of four H atoms at the hollow sites adjacent to the segregated Pt within the terrace and the three hollow sites and one bridge site adjacent to the segregated Pt in the step edge, as illustrated in Fig. 4(c). These calculations demonstrate the initially preferred Pt segregation to the step edge over the terrace site, consistent with the experimental observations shown in Figs. 1 and 2.

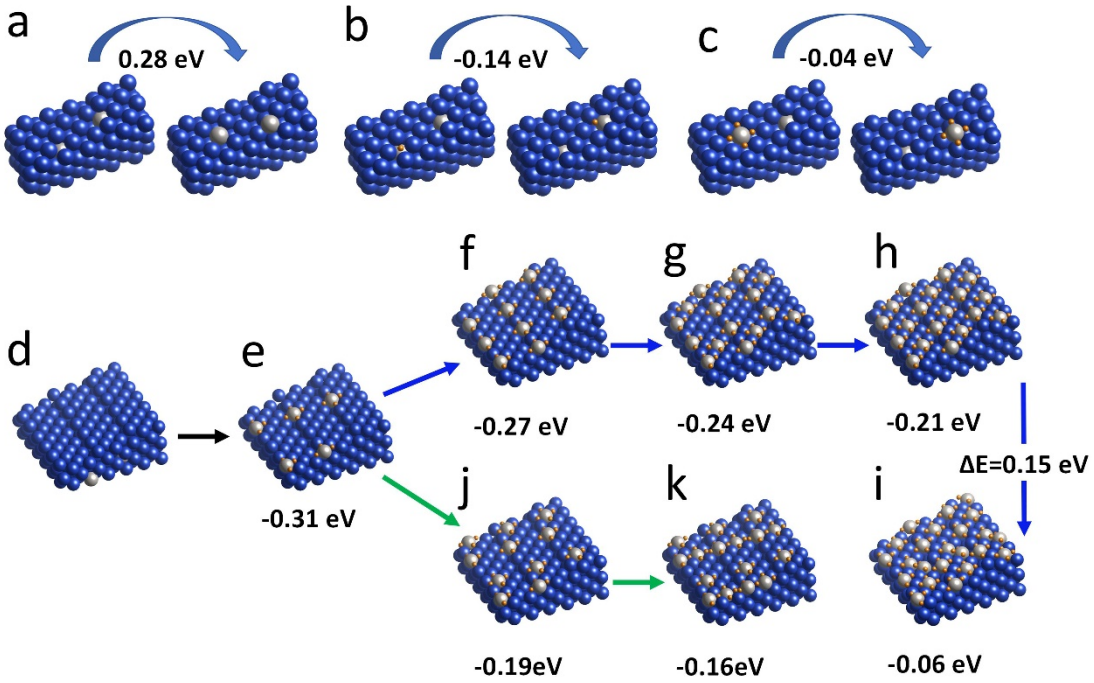

Fig. 4: DFT modeling of H adsorption-induced Pt segregation on a stepped (410) surface. (a) Energy difference between two Pt atoms located in the subsurface and their segregation to the step edge and terrace on the pristine surface. (b) Energy difference for H adsorption at the terrace hollow site right above the subsurface Pt, compared to the hollow site near subsurface Pt along the step edge. (c) Energy difference for Pt segregation to the terrace, with H adsorption at the four adjacent hollow sites of the segregated Pt atom, versus Pt segregation to the step edge, with H adsorption at the adjacent hollow and bridge sites of the segregated Pt atom. (d-k) Energy landscape illustrating the sequential process of H adsorption and resulting Pt segregation on the (410) facet, initially at the step edge, and subsequently propagating to sites within the terrace.

We then identify the pathway leading to the population of segregated Pt atoms from the step edge to the terrace region of the (410) facet. As presented in Figs. 4(d, e), segregation of the first Pt atom to the step edge along with H adsorption at the adjacent hollow and bridge sites is energetically favorable. After the first Pt atom, it is observed that its next nearest neighbor within the step edge is the most favorable site for H adsorption-induced segregation of the second Pt atom (Fig. 4(f)), resulting in 50% of Pt occupancy in the step edge and aligning with the simulated HRTEM image in Fig. 1(d). Subsequently, it is found that the H adsorption-induced segregation of the third and fourth Pt atoms occurs preferentially at the alternative lattice sites of the atom column in the middle of the terrace. This results in 50%Pt occupancy within the column (Figs. 4(h)) and corresponds to the Pt-segregated structure illustrated in Fig. 2(e).

Alternatively, another Pt segregation pathway can be identified from the DFT modeling. As depicted in Fig. 4(j), the second Pt can also segregate to the atom column adjacent to the step edge. Subsequently, the third Pt segregates onto the next adjacent atom column, ultimately forming three Pt-containing neighboring atom columns with 25% Pt occupancy in each column (Fig. 4(k)), corresponding to the Pt-segregated structure illustrated in Fig. 3(f). The segregation energy calculations indicate that this Pt segregation path (Figs. 4(e, j, k) is slightly less favorable, but with a minimal difference, compared to the path depicted in Figs. 4(e-h). This leads to the coexistence of the two Pt-segregated structures depicted in Figs. 3(e, f), which aligns well with the simulated and experimental HRTEM images (Fig. 3(d)).

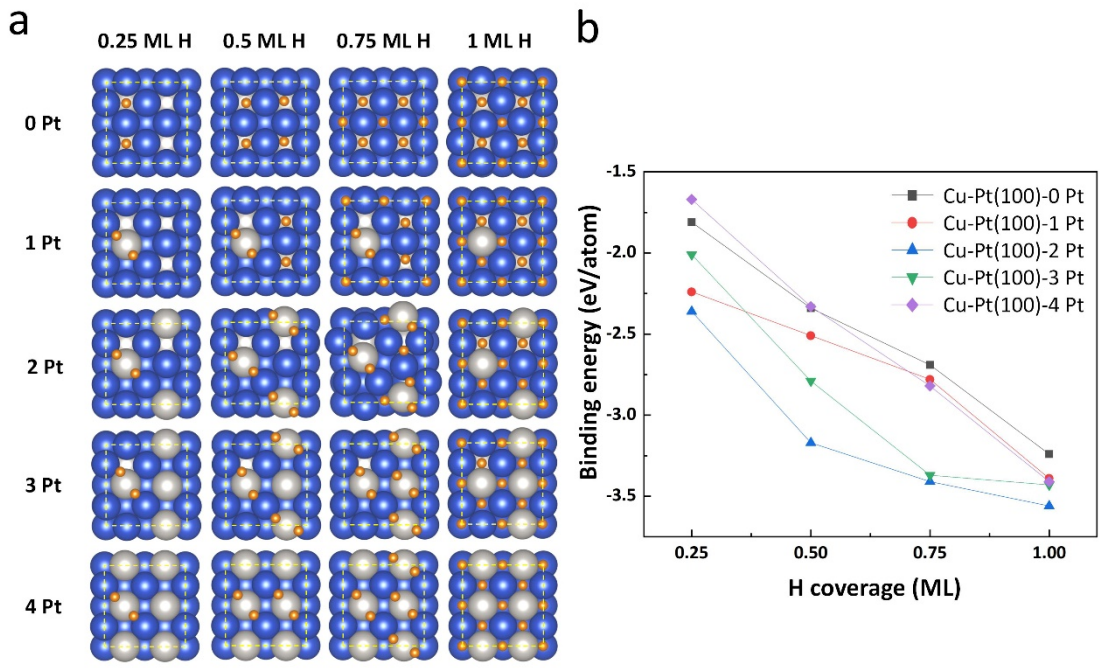

Fig. 5: DFT modeling of H adsorption-induced Pt segregation on the (100) surface. (a) Top view of the surface sites for H adsorption and the resulting Pt segregation at different H coverages. (b) Calculated binding energy per H atom at the most stable adsorption sites as a function of the H coverage and the number of segregated Pt atoms.

We then model the effect of H adsorption on Pt segregation to the flat (100) surface, resulting in the formation of the p(2×2) arrangement of segregated Pt atoms. As shown in Fig. 5(a), the simulation supercells contain four Pt atoms initially positioned at the lattice sites in the second layer of the pristine Cu-terminated surface. We systematically assess the binding energy of H as a function of the surface coverage of both adsorbed H and segregated Pt,

including Cu(100)-0Pt, Cu(100)-1Pt, Cu(100)-2Pt, Cu(100)-3Pt, and Cu(100)-4Pt configurations, with the H coverages of 0.25, 0.5, 0.75, and 1 monolayer (ML). Here, the terms 0Pt, 1Pt, 2Pt, 3Pt and 4Pt denote the number of segregated Pt atoms from the subsurface, while the surface coverage of H is defined as the ratio of the number of adsorbed H atoms to all potential adsorption sites within the unit cell. The computation results, displayed in Fig. 5(b), reveal that the H binding energy becomes increasingly negative with higher H coverage, indicating enhanced stability.

Notably, the Cu(100)-2Pt structure consistently exhibits the most negative H binding energy across various H coverages up to 1 ML, indicating its preference as the most stable configuration compared to others. This finding aligns with experimental result observed from in-situ TEM imaging, as depicted in Figs. 3(b), where the detected p(2×2) ordering of segregated Pt atoms on the (100) surface corresponds to the Cu(100)-2Pt structure with 25% of Pt occupancy of the unit cell. Further analysis of the Cu(100)-2Pt configuration in Fig. 5(a) reveals the evolution of surface adsorption sites for H. At H coverages of 0.25 and 0.5 ML, H atoms tend to adsorb favorably at the bridge sites between the segregated Pt atom and its adjacent Cu atoms. With an increase in H coverage to 0.75, some H atoms are observed to adsorb at the shifted bridge sites formed between the segregated Pt atom and its two adjacent Cu atoms. Finally, at a coverage of 1 ML H, all H atoms are found to adsorb onto the hollow sites formed between the segregated Pt atoms and the surrounding Cu atoms. Fig. 5(b) displays the corresponding H binding energy at the various surface sites, indicating that the Cu-Pt(100)-2Pt surface structure exhibits the most negative binding energy for H adsorption. This makes it the most stable configuration across the different surface coverages of adsorbed H.

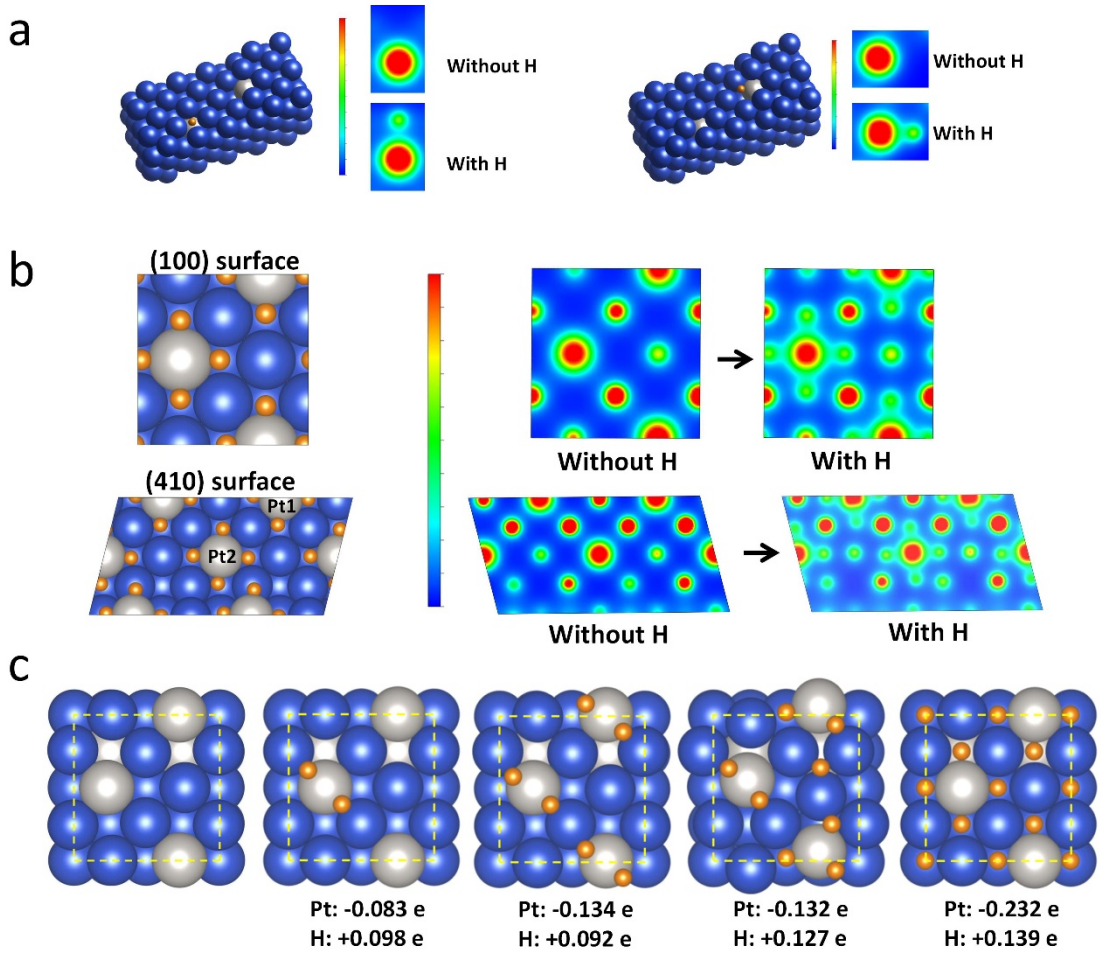

Fig. 6: Electronic analysis of H-adsorption-induced surface segregation of Pt. (a) H adsorption at the terrace hollow site directly above the subsurface Pt and at the hollow site near the subsurface Pt along the step edge, accompanied by a comparison of the electron density maps with and without adsorbed H. (b) Top views of the most stable H-adsorbed structures for the (100) and (410) surfaces, including a comparison of the electron density maps for the structures with and without adsorbed H. Pt1 and Pt2 correspond to the Pt atoms at the step edge and within the terrace of the (410) surface, respectively. (c) Top views of the (100)-2Pt structures, along with the average Bader charge of the segregated Pt as a function of the surface coverage of adsorbed H. The red and blue colors in (a, b) indicate the high and low electron density, respectively.

Finally, we perform an electronic structure analysis to deepen our understanding of H-adsorption-induced surface segregation of Pt. Fig. 6(a) presents the structure and corresponding electron density maps of a single Pt atom with and without the adsorbed H on the terrace and along the step edge. At the terrace site, the electron density around the subsurface Pt shows little overlap with the adsorbed H at the hollow site right above it, indicating a weak interaction that does not significantly drive surface segregation of the subsurface Pt. In contrast, for the

subsurface Pt along the step edge, the electron density map reveals notable overlap with the adsorbed H at the hollow site above it. This suggests a stronger bonding interaction between Pt and H, resulting in a partial transfer of electrons from the Pt atom to adsorbed H. This electronic interaction provides a greater driving force for surface segregation of the sub-surface Pt along the step edge. This observation aligns with our HRTEM imaging (Figs. 1, 2), which shows that Pt preferentially segregates along the step edges before migrating to the (100) terrace region.

Fig. 6(b) illustrates the surface structures and corresponding electronic density maps of the most stable configurations of the Pt-segregated (100) and (410) surfaces at 1 ML surface coverage of adsorbed H. For comparison, the electron density maps for the surfaces without adsorbed H are also included to show the differences. In the absence of adsorbed H, the electron density on both the (100) and (410) surfaces is mainly concentrated around the Pt atoms. However, when H atoms are adsorbed onto the adjacent hollow sites, the electron density around the Pt atoms spreads towards the adsorbed H atoms, showing significant overlap. This indicates a transfer of electrons from the Pt atoms to the H atoms, leading to the stabilized structures for the (100) and (410) with saturated Pt coverage, consistent with the TEM observations shown in Fig. 3.

Fig. 6(c) presents the Bader charge analysis of the segregated Pt and H in the Cu-Pt(100)-2Pt surface structure, which is the most stable configuration across various surface coverages of adsorbed H (Fig. 5(b)). In this analysis, we do not consider the electron gain or loss of Cu, as it does not interact significantly with H[6, 69]. The analysis reveals that the surface-segregated Pt tends to lose more electrons as the surface coverage of adsorbed H increases. Specifically, compared to the surface without adsorbed H, the average Bader charge of the Pt atoms decreases by 0.232 e at 1 ML of H coverage. Furthermore, the Bader charge for each adsorbed H is positive, indicating that the H atoms gain electrons when interacting with the segregated Pt. For instance, at a coverage of 0.25 ML, the average Bader charge of the adsorbed H is 0.098 e, while at 1 ML coverage, each H gains an average of 0.139 e from the segregated Pt. This trend aligns with the electron density maps (Fig. 6(b)), which shows the redistribution of the electron density from the Pt atom toward the adjacent H atoms.

4. DISCUSSION

The E-TEM imaging, complemented by DFT modeling, provides atomic-scale insights into the structure and composition dynamics in the topmost surface layer of a dilute Cu(Pt) alloy under H_2 atmosphere and elevated temperatures. Here, the chemical affinity of H for Pt not only drives the surface segregation of Pt but also promotes an ordered distribution of segregated Pt atoms in the surface layer. Understanding such surface segregation in reactive environments is crucial for various applications, particularly in heterogeneous catalysis, where the distribution of surface elements can significantly influence reaction pathways and catalytic efficiency. Additionally, the stability of alloys in these reactive environments is heavily influenced by surface segregation. For instance, under corrosive or high-temperature conditions, segregation can lead to the formation of unstable surface phases or deplete the alloy of crucial components, thereby compromising its mechanical and chemical stability.

However, in-situ TEM is limited in its ability to measure the surface chemistry, as it cannot distinguish between different chemical states of the alloy components simultaneously. Furthermore, the sample size and geometry suitable for in-situ TEM may not fully represent the behavior of bulk materials or complex surface morphologies seen in larger samples. To achieve a comprehensive understanding of surface segregation, complementary techniques such as XPS are necessary. XPS can provide detailed information on chemical states and elemental composition at the surface. Nonetheless, integrating XPS with TEM is challenging due to technical constraints, such as the need for extended single crystals for XPS or a collection of nanoparticles. However, obtaining an extended dilute Cu-5at.%Pt(100) single crystal for XPS measurements is not feasible. Additionally, the surface segregation phenomena observed in our in-situ TEM experiments involve co-existing (100) and (410) facets, making it challenging to correlate with XPS data obtained from a single surface orientation on extended crystals. Similarly, nanoparticle samples typically lack well-developed facets, further hindering meaningful comparison. Future studies bridging the material gap between E-TEM and complementary techniques like XPS require advances in sample preparation, analysis

techniques, and instrument design for overcoming current limitations. Achieving this will provide a more complete picture of material behavior under realistic conditions – such as high temperatures and reactive gases – thereby enhancing our understanding of how alloys perform in actual operating environments.

5. CONCLUSIONS

Using environmental TEM, we monitor H adsorption-induced surface segregation of Pt in a dilute Cu(Pt) solid solution. Through direct comparison of the flat (100) and stepped (410) surfaces under identical conditions of elevated temperature and H_2 atmosphere, we observed that Pt segregation initially occurs at the step edges. Subsequently, it propagates to the terrace sites, resulting in ~22% of Pt occupancy of the stepped facet as the H coverage increases. In contrast, H adsorption-induced Pt segregation on the (100) surface initially manifests as isolated Pt atoms, which then self-order into a p(2×2) structure with 25% of Pt occupancy of the surface sites with the increased H coverage. These observations provide mechanistic insights into the dynamic evolution of surface composition and structure of the Cu(Pt) alloy in response to environmental stimuli. The results are of practical implications, especially in the field of heterogeneous catalysis, where the formation of single-atom alloys is particularly attractive for PGM catalysts. Understanding how these catalysts respond to environmental factors like H adsorption and elevated temperatures aids in optimizing their performance and designing more efficient catalytic systems.

Acknowledgements: This work was supported by the National Science Foundation (NSF) under the NSF Collaborative Research Award grant DMR 1905422 and 1905572. This research used the Electron Microcopy Facilities and the Theory and Computation resources of the Center for Functional Nanomaterials, which is a U.S. DOE Office of Science Facility, at Brookhaven National Laboratory under Contract No. DE-SC0012704.

References:

(1) Zafeiratos, S.; Piccinin, S.; Teschner, D. Alloys in Catalysis: Phase Separation and Surface Segregation Phenomena in Response to the Reactive Environment. *Catal. Sci. Technol.* **2012,** *2,* 1787–1801.
(2) Liao, H.; Fisher, A.; Xu, Z. J. Surface Segregation in Bimetallic Nanoparticles: A Critical Issue in Electrocatalyst Engineering. *Small* **2015,** *11,* 3221–3246.
(3) Ferrari, A.; Körmann, F. Surface Segregation in Cr–Mn–Fe–Co–Ni High Entropy Alloys. *Appl. Surf. Sci.* **2020,** *533,* 147471.
(4) Zou, L.; Yang, C.; Lei, Y.; Zakharov, D.; Wiezorek, J. M. K.; Su, D.; Yin, Q.; Li, J.; Liu, Z.; Stach, E. A.; et al. Dislocation Nucleation Facilitated by Atomic Segregation. *Nat. Mater.* **2018**, *17*, 56-63.
(5) Zou, L.; Saidi, W. A.; Lei, Y.; Liu, Z.; Li, J.; Li, L.; Zhu, Q.; Zakharov, D.; Stach, E. A.; Yang, J. C.; et al. Segregation Induced Order-Disorder Transition in Cu(Au) Surface Alloys. *Acta Mater.* **2018,** *154,* 220–227.
(6) Li, C.; Liu, Q.; Boscoboinik, J. A.; Zhou, G. Tuning the Surface Composition of Cu_3Au Binary Alloy. *Phys. Chem. Chem. Phys.* **2020,** *22,* 3379–3389.
(7) Meng, J.; Zhu, B.; Gao, Y. Surface Composition Evolution of Bimetallic Alloys under Reaction Conditions. *J. Phys. Chem. C* **2019,** *123,* 28241–28247.
(8) Wang, C.-M.; Genc, A.; Cheng, H.; Pullan, L.; Baer, D. R.; Bruemmer, S. M. In-Situ TEM Visualization of Vacancy Injection and Chemical Partition During Oxidation of Ni-Cr Nanoparticles. *Sci. Rep.* **2014,** *4,* 3683.
(9) van Spronsen, M. A.; Daunmu, K.; O'Connor, C. R.; Egle, T.; Kersell, H.; Oliver-Meseguer, J.; Salmeron, M. B.; Madix, R. J.; Sautet, P.; Friend, C. M. Dynamics of Surface Alloys: Rearrangement of Pd/Ag(111) Induced by CO and O_2. *J. Phys. Chem. C* **2018,** *123,* 8312–8323.
(10) Boyes, E. D.; LaGrow, A. P.; Ward, M. R.; Mitchell, R. W.; Gai, P. L. Single Atom Dynamics in Chemical Reactions. *Acc. Chem. Res.* **2020,** *53,* 390–399.
(11) Gao, W.; Hood, Z. D.; Chi, M. Interfaces in Heterogeneous Catalysts: Advancing Mechanistic Understanding through Atomic-Scale Measurements. *Acc. Chem. Res.* **2017,** *50,* 787–795.
(12) Taleblou, M.; Camellone, M. F.; Fabris, S.; Piccinin, S. Oxidation of Gas-Phase and Supported Pt Nanoclusters: An Ab Initio Investigation. *J. Phys. Chem. C* **2022,** *126,* 10880–10888.
(13) Zugic, B.; Wang, L.; Heine, C.; Zakharov, D. N.; Lechner, B. A.; Stach, E. A.; Biener, J.; Salmeron, M.; Madix, R. J.; Friend, C. M. Dynamic Restructuring Drives Catalytic Activity on Nanoporous Gold–Silver Alloy Catalysts. *Nat. Mater.* **2017,** *16,* 558–564.
(14) Li, X.; Zhao, J.; Su, D. Structural Changes of Intermetallic Catalysts under Reaction Conditions. *Small Struct.* **2021,** *2,* 2100011.
(15) Pan, Y.-T.; Wu, J.; Yin, X.; Yang, H. In Situ ETEM Study of Composition Redistribution in Pt–Ni Octahedral Catalysts for Electrochemical Reduction of Oxygen. *AIChE J.* **2016,** *62,* 399–407.

(16) Liu, S.; Chen, Y.; An, Z.; Zhao, J.; Lu, H.; Jiao, Y.; Xie, L.; Li, A.; Han, X. Microstructure and Oxidation of NiCr Alloys Studied by Analytical In Situ Environmental TEM. *Corros. Sci.* **2023,** *224,* 111525.
(17) Sun, X.; Wu, D.; Zou, L.; House, S. D.; Chen, X.; Li, M.; Zakharov, D. N.; Yang, J. C.; Zhou, G. Dislocation-Induced Stop-and-Go Kinetics of Interfacial Transformations. *Nature* **2022**, *607*, 708-713.
(18) Zhang, J.; Qu, X.; Han, Y.; Shen, L.; Yin, S.; Li, G.; Jiang, Y.; Sun, S. Engineering PtRu Bimetallic Nanoparticles with Adjustable Alloying Degree for Methanol Electrooxidation: Enhanced Catalytic Performance. *Appl. Catal. B* **2020**, *263*, 118345.
(19) Fan, J.; Du, H.; Zhao, Y.; Wang, Q.; Liu, Y.; Li, D.; Feng, J. Recent Progress on Rational Design of Bimetallic Pd Based Catalysts and Their Advanced Catalysis. *ACS Catal.* **2020**, *10*, 13560-13583.
(20) Jo, D. Y.; Lee, M. W.; Kim, C. H.; Choung, J. W.; Ham, H. C.; Lee, K.-Y. Interplay of Ligand and Strain Effects in CO Adsorption on Bimetallic Cu/M (M = Ni, Ir, Pd, and Pt) Catalysts from First-Principles: Effect of Different Facets on Catalysis. *Catal. Today* **2021**, *359*, 57-64.
(21) Aich, P.; Wei, H.; Basan, B.; Kropf, A. J.; Schweitzer, N. M.; Marshall, C. L.; Miller, J. T.; Meyer, R. Single-Atom Alloy Pd–Ag Catalyst for Selective Hydrogenation of Acrolein. *J. Phys. Chem. C* **2015**, *119*, 18140-18148.
(22) Pei, G. X.; Liu, X. Y.; Wang, A.; Li, L.; Huang, Y.; Zhang, T.; Lee, J. W.; Jang, B. W. L.; Mou, C.-Y. Promotional Effect of Pd Single Atoms on Au Nanoparticles Supported on Silica for the Selective Hydrogenation of Acetylene in Excess Ethylene. *New J. Chem.* **2014**, *38*, 2043-2051.
(23) Pei, G. X.; Liu, X. Y.; Wang, A.; Lee, A. F.; Isaacs, M. A.; Li, L.; Pan, X.; Yang, X.; Wang, X.; Tai, Z.; et al. Ag Alloyed Pd Single-Atom Catalysts for Efficient Selective Hydrogenation of Acetylene to Ethylene in Excess Ethylene. *ACS Catal.* **2015**, *5*, 3717-3725.
(24) Haruta, M. Size- and Support-Dependency in the Catalysis of Gold. *Catal. Today* **1997**, *36*, 153-166.
(25) Campbell, C. T.; Parker, S. C.; Starr, D. E. The Effect of Size-Dependent Nanoparticle Energetics on Catalyst Sintering. *Science* **2002**, *298*, 811-814.
(26) Li, W.; Guo, Z.; Yang, J.; Li, Y.; Sun, X.; He, H.; Li, S.; Zhang, J. Advanced Strategies for Stabilizing Single-Atom Catalysts for Energy Storage and Conversion. *Electrochem. Energy Rev.* **2022**, *5*, 9.
(27) Liu, L.; Chen, T.; Chen, Z. Understanding the Dynamic Aggregation in Single-Atom Catalysis. *Adv. Sci.* **2024**, *11*, 2308046.
(28) Liu, J.; Bunes, B. R.; Zang, L.; Wang, C. Supported Single-Atom Catalysts: Synthesis, Characterization, Properties, and Applications. *Environ. Chem. Lett.* **2018**, *16*, 477-505.
(29) Qin, R.; Liu, P.; Fu, G.; Zheng, N. Strategies for Stabilizing Atomically Dispersed Metal Catalysts. *Small Methods* **2018**, *2*, 1700286.

(30) Kyriakou, G.; Boucher, M. B.; Jewell, A. D.; Lewis, E. A.; Lawton, T. J.; Baber, A. E.; Tierney, H. L.; Flytzani-Stephanopoulos, M.; Sykes, E. C. H. Isolated Metal Atom Geometries as a Strategy for Selective Heterogeneous Hydrogenations. *Science* **2012**, *335*, 1209-1212.
(31) Lucci, F. R.; Liu, J.; Marcinkowski, M. D.; Yang, M.; Allard, L. F.; Flytzani-Stephanopoulos, M.; Sykes, E. C. H. Selective Hydrogenation of 1,3-Butadiene on Platinum–Copper Alloys at the Single-Atom Limit. *Nat. Commun.* **2015**, *6*, 8550.
(32) Muir, M.; Trenary, M. Adsorption of CO to Characterize the Structure of a Pd/Ag (111) Single-Atom Alloy Surface. *J. Phys. Chem. C* **2020**, 124, 14722–14729.
(33) Zhang, T.; Walsh, A. G.; Yu, J.; Zhang, P. Single-Atom Alloy Catalysts: Structural Analysis, Electronic Properties and Catalytic Activities. *Chem. Soc. Rev.* **2021**, *50*, 569-588.
(34) Simonovis, J. P.; Hunt, A.; Palomino, R. M.; Senanayake, S. D.; Waluyo, I. Enhanced Stability of Pt–Cu Single-Atom Alloy Catalysts: In Situ Characterization of the Pt/Cu (111) Surface in an Ambient Pressure of CO. *J. Phys. Chem. C* **2018**, 122, 4488–4495.
(35) Wang, Q.; Zhu, B.; Tielens, F.; Guesmi, H. Single Metal Atoms Embedded in the Surface of Pt Nanocatalysts: The Effect of Temperature and Hydrogen Pressure. *Catalysts* **2022**, *12*, 1669.
(36) Liu, L.; Corma, A. Confining Isolated Atoms and Clusters in Crystalline Porous Materials for Catalysis. *Nat. Rev. Mater.* **2021**, *6*, 244-263.
(37) Wang, L.; Wang, L.; Meng, X.; Xiao, F.-S. New Strategies for the Preparation of Sinter-Resistant Metal-Nanoparticle-Based Catalysts. *Adv. Mater.* **2019**, *31*, 1901905.
(38) Kim, I. S.; Li, Z.; Zheng, J.; Platero-Prats, A. E.; Mavrandonakis, A.; Pellizzeri, S.; Ferrandon, M.; Vjunov, A.; Gallington, L. C.; Webber, T. E.; et al. Sinter-Resistant Platinum Catalyst Supported by Metal–Organic Framework. *Angew. Chem. Int. Ed.* **2018**, *57*, 909-913.
(39) Lin, T.; Wang, H.; Cui, C.; Liu, W.; Li, G. Recent Advances on Confining Noble Metal Nanoparticles Inside Metal-Organic Frameworks for Hydrogenation Reactions. *Chem. Res. Chin. Univ.* **2022**, *38*, 1309-1323.
(40) Yang, M.; Li, S.; Wang, Y.; Herron, J. A.; Xu, Y.; Allard, L. F.; Lee, S.; Huang, J.; Mavrikakis, M.; Flytzani-Stephanopoulos, M. Catalytically Active Au-O (OH) x-Species Stabilized by Alkali Ions on Zeolites and Mesoporous Oxides. *Science* **2014**, *346*, 1498-1501.
(41) Shin, J.; Lee, Y. J.; Jan, A.; Choi, S. M.; Park, M. Y.; Choi, S.; Hwang, J. Y.; Hong, S.; Park, S. G.; Chang, H. J.; et al. Highly Active and Thermally Stable Single-Atom Catalysts for High-Temperature Electrochemical Devices. *Energy Environ. Sci.* **2020**, *13*, 4903-4920.
(42) Qiao, B.; Wang, A.; Yang, X.; Allard, L. F.; Jiang, Z.; Cui, Y.; Liu, J.; Li, J.; Zhang, T. Single-Atom Catalysis of CO Oxidation Using Pt_1/FeO_x. *Nat. Chem.* **2011**, *3*, 634-641.

(43) Pereira-Hernández, X. I.; DeLaRiva, A.; Muravev, V.; Kunwar, D.; Xiong, H.; Sudduth, B.; Engelhard, M.; Kovarik, L.; Hensen, E. J. M.; Wang, Y.; et al. Tuning Pt-CeO_2 Interactions by High-Temperature Vapor-Phase Synthesis for Improved Reducibility of Lattice Oxygen. *Nat. Commun.* **2019**, *10*, 1358.
(44) Hannagan, R. T.; Giannakakis, G.; Flytzani-Stephanopoulos, M.; Sykes, E. C. H. Single-Atom Alloy Catalysis. *Chem. Rev.* **2020**, *120*, 12044-12088.
(45) Lucci, F. R.; Lawton, T. J.; Pronschinske, A.; Sykes, E. C. H. Atomic Scale Surface Structure of Pt/Cu (111) Surface Alloys. *J. Phys. Chem. C* **2014**, *118*, 3015-3022.
(46) Zhang, L.; Long, R.; Zhang, Y.; Duan, D.; Xiong, Y.; Zhang, Y.; Bi, Y. Direct Observation of Dynamic Bond Evolution in Single-Atom Pt/C_3N_4 Catalysts. *Angew. Chem.* **2020**, *132*, 6283-6288.
(47) Chen, Z.; Zhang, P. Electronic Structure of Single-Atom Alloys and Its Impact on the Catalytic Activities. *ACS Omega* **2022**, *7*, 1585-1594.
(48) Li, X.; Yang, X.; Zhang, J.; Huang, Y.; Liu, B. In situ/operando Techniques for Characterization of Single-Atom Catalysts. *ACS Catal.* **2019**, *9*, 2521-2531.
(49) Kresse, G.; Hafner, J. Ab Initio Molecular Dynamics for Liquid Metals. *Phys. Rev. B* **1993**, *47*, 558.
(50) Kresse, G.; Hafner, J. Ab Initio Molecular-Dynamics Simulation of the Liquid-Metal–Amorphous-Semiconductor Transition in Germanium. *Phys. Rev. B* **1994**, *49*, 14251.
(51) Kresse, G.; Furthmüller, J. Efficiency of Ab-initio Total Energy Calculations for Metals and Semiconductors Using a Plane-Wave Basis Set. *Comput. Mater. Sci.* **1996**, *6*, 15-50.
(52) Perdew, J. P.; Burke, K.; Ernzerhof, M. Generalized Gradient Approximation Made Simple. *Phys. Rev. Lett.* **1996**, *77*, 3865.
(53) Kresse, G.; Joubert, D. From Ultrasoft Pseudopotentials to the Projector Augmented-Wave Method. *Phys. Rev. B* **1999**, *59*, 1758.
(54) Monkhorst, H. J.; Pack, J. D. Special Points for Brillouin-Zone Integrations. *Phys. Rev. B* **1976**, *13*, 5188.
(55) Zhang, S.; Wang, R.; Zhang, X.; Zhao, H. Recent Advances in Single-Atom Alloys: Preparation Methods and Applications in Heterogeneous Catalysis. *RSC Adv.* **2024**, *14*, 3936-3951.
(56) Zhang, L.; Banis, M. N.; Sun, X. Single-Atom Catalysts by the Atomic Layer Deposition Technique. *Natl. Sci. Rev.* **2018**, *5*, 628-630.
(57) Li, C.; Zhu, Y.; Wu, D.; Boscoboinik, J. A.; Zhou, G. Effect of Surface Segregation on the Oxidation Resistance of Cu_3Pt(100). *Phys. Rev. Mater.* **2022**, *6*, 025801.
(58) Shen, Y. G.; O'Connor, D. J.; Wandelt, K.; MacDonald, R. J. Studies of Surface Composition and Structure of Cu_3Pt(111) by Low Energy Alkali Ion Scattering. *Surf. Sci.* **1995**, *328*, 21-31.

(59) Shen, Y. G.; O'Connor, D. J.; Wandelt, K. The Surface Composition, Structure and Oxygen-Induced (2×1) Reconstruction of Cu_3Pt(110). *Surf. Sci.* **1998**, *410*, 1-14.
(60) Shen, Y. G.; O'Connor, D. J.; Wandelt, K. Composition and Structure of Cu_3Pt(001): a (1×1) Cu Termination with c (2×2) Underlayer Ordering. *Surf. Sci.* **1998**, *406*, 23-31.
(61) Greeley, J.; Mavrikakis, M. Surface and Subsurface Hydrogen: Adsorption Properties on Transition Metals and Near-Surface Alloys. *J. Phys. Chem. B* **2005**, *109*, 3460-3471.
(62) Yasumori, I.; Momma, N.; Kiyomiya, M. Mechanism of Hydrogen Adsorption and Hydrogen-Deuterium Equilibration on Copper Surface. *Jpn. J. Appl. Phys.* **1974**, *13*, 485.
(63) Poelsema, B.; Lenz, K.; Comsa, G. The Dissociative Adsorption of Hydrogen on Pt(111): Actuation and Acceleration by Atomic Defects. *J. Chem. Phys.* **2011**, *134*, 074703.
(64) Christmann, K.; Ertl, G.; Pignet, T. Adsorption of Hydrogen on a Pt(111) Surface. *Surf. Sci.* **1976**, *54*, 365-392.
(65) Groot, I. M. N.; Kleyn, A. W.; Juurlink, L. B. F. Separating Catalytic Activity at Edges and Terraces on Platinum: Hydrogen Dissociation. *J. Phys. Chem. C* **2013**, *117*, 9266-9274.
(66) Simonovis, J. P.; Hunt, A.; Waluyo, I. In situ Ambient Pressure XPS Study of Pt/Cu(111) Single-Atom Alloy in Catalytically Relevant Reaction Conditions. *J. Phys. D: Appl. Phys.* **2021**, *54*, 194004.
(67) Andersson, K. J.; Calle-Vallejo, F.; Rossmeisl, J.; Chorkendorff, I. Adsorption Driven Surface Segregation of the Less Reactive Alloy Component. *J. Am. Chem. Soc.* **2009**, *131*, 2404-2407.
(68) Schurmans, M.; Luyten, J.; Creemers, C.; Declerck, R.; Waroquier, M. Surface Segregation in CuPt Alloys by Means of an Improved Modified Embedded Atom Method. *Phys. Rev. B* **2007**, *76*, 174208.
(69) Li, J.; Zhang, S.; Li, C.; Zhu, Y.; Boscoboinik, J. A.; Tong, X.; Sadowski, J. T.; Wang, G.; Zhou, G. Coupling between Bulk Thermal Defects and Surface Segregation Dynamics. *Phys. Rev. B* **2021,** *104,* 085408.

TOC Graphic

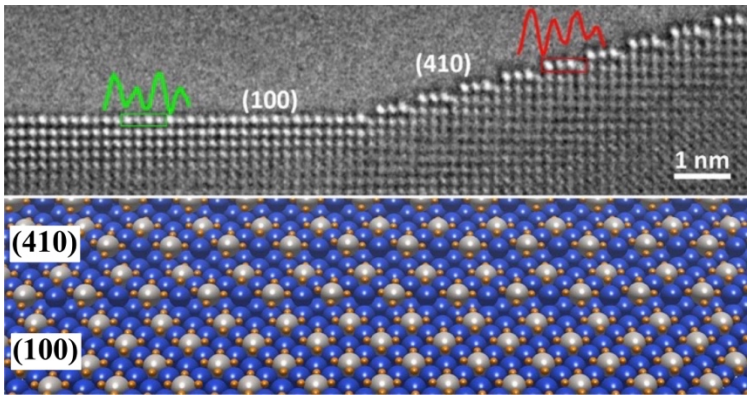

1